

^{18}F -FEAC and ^{18}F -FEDAC: PET of the Monkey Brain and Imaging of Translocator Protein (18 kDa) in the Infarcted Rat Brain

Joji Yui¹, Jun Maeda¹, Katsushi Kumata¹, Kazunori Kawamura¹, Kazuhiko Yanamoto¹, Akiko Hatori¹, Tomoteru Yamasaki¹, Nobuki Nengaki^{1,2}, Makoto Higuchi¹, and Ming-Rong Zhang¹

¹Molecular Imaging Center, National Institute of Radiological Sciences, Chiba, Japan; and ²SHI Accelerator Service Co. Ltd., Tokyo, Japan

We evaluated two ^{18}F -labeled PET ligands, *N*-benzyl-*N*-ethyl-2-[7,8-dihydro-7-(2- ^{18}F -fluoroethyl)-8-oxo-2-phenyl-9H-purin-9-yl]acetamide (^{18}F -FEAC) and *N*-benzyl-*N*-methyl-2-[7,8-dihydro-7-(2- ^{18}F -fluoroethyl)-8-oxo-2-phenyl-9H-purin-9-yl]acetamide (^{18}F -FEDAC), by investigating their kinetics in the monkey brain and by performing in vitro and in vivo imaging of translocator protein (18 kDa) (TSPO) in the infarcted rat brain.

Methods: Dissection was used to determine the distribution of ^{18}F -FEAC and ^{18}F -FEDAC in mice, whereas PET was used for a monkey. With each ^{18}F -ligand, in vitro autoradiography and small-animal PET were performed on infarcted rat brains.

Results: ^{18}F -FEAC and ^{18}F -FEDAC had a high uptake of radioactivity in the heart, lung, and other TSPO-rich organs of mice. In vitro autoradiography showed that the binding of each ^{18}F -ligand significantly increased on the ipsilateral side of rat brains, compared with the contralateral side. In a small-animal PET study, PET summation images showed the contrast of radioactivity between ipsilateral and contralateral sides. Pretreatment with TSPO ligands *N*-benzyl-*N*-ethyl-2-(7-methyl-8-oxo-2-phenyl-7,8-dihydro-9H-purin-9-yl)acetamide (AC-5216) or (*R*)-*N*-methyl-*N*-(1-methylpropyl)-1-(2-chlorophenyl)isoquinoline-3-carboxamide (PK11195) diminished the difference in uptake between the 2 sides. The PET study showed that each ^{18}F -ligand had uptake and distribution patterns in the monkey brain similar to those of ^{11}C -AC-5216. After injection into the monkey during PET, the uptake of each ^{18}F -ligand in the brain decreased over time whereas ^{11}C -AC-5216 did not. In the brain homogenate of mice, the percentage of the fraction corresponding to intact ^{18}F -FEAC and ^{18}F -FEDAC was 68% and 75% at 30 min after injection. In monkey plasma, each ^{18}F -ligand was scarcely metabolized until the end of the PET scan. **Conclusion:** ^{18}F -FEAC and ^{18}F -FEDAC produced in vitro and in vivo signals allowing visualization of the increase in TSPO expression in the infarcted rat brain. The kinetics of both ^{18}F -ligands in the monkey brain and tolerance for in vivo metabolism suggested their usefulness for imaging studies of TSPO in primates.

Key Words: translocator protein (18 kDa); ^{18}F -FEAC; ^{18}F -FEDAC; ischemia; infarction

J Nucl Med 2010; 51:1301–1309

DOI: 10.2967/jnumed.109.072223

The translocator protein (18 kDa) (TSPO) (1), formerly known as peripheral-type benzodiazepine receptor, is widely distributed in peripheral tissues and the brain (2,3). In the brain, TSPO is located mainly in glial cells, and TSPO expression was increased in microglial cells activated by brain injury or neuroinflammation (4–7). Neuropathologic evidence has demonstrated that an increase in TSPO and concurrent microglial and astroglial activation accompanies the neurodegenerative process in Alzheimer disease (7–9). These findings motivated the development of imaging probes labeled by positron-emitting radionuclides and have enabled visualization of the distribution and change in TSPO induced by microglial activation in normal and abnormal brains of humans and animals (10–18).

^{11}C -labeled (*R*)-*N*-methyl-*N*-(1-methylpropyl)-1-(2-chlorophenyl)isoquinoline-3-carboxamide (PK11195) was the first PET ligand used for clinical imaging of TSPO (19). However, ^{11}C -PK11195 has several limitations, such as relatively low brain uptake, high nonspecific binding, high plasma protein binding, and very high lipophilicity (20). To precisely characterize TSPO with an improved PET ligand, several new ligands labeled with ^{11}C or ^{18}F have been reported (10,11). Of these ligands, ^{11}C -labeled *N,N*-diethyl-2-[2-(4-methoxyphenyl)-5,7-dimethylpyrazolo[1,5- α]pyrimidin-3-yl]acetamide (DPA-713) and ^{18}F -labeled *N,N*-diethyl-2-(2-(4-(2-fluoroethoxy)phenyl)-5,7-dimethylpyrazolo[1,5- α]pyrimidin-3-yl)acetamide (DPA-714) are promising PET ligands with potent binding affinity and suitable kinetics in rodent and primate brains for TSPO imaging (14,15,17,18). We have developed *N*-(2- ^{11}C ,5-dimethoxybenzyl)-*N*-(5-fluoro-2-phenoxyphenyl)acetamide (^{11}C -DAA1106), *N*-(5-fluoro-2-phenoxyphenyl)-*N*-(2- ^{18}F -fluoroethyl-5-methoxybenzyl)acetamide (^{18}F -

Received Oct. 31, 2009; revision accepted May. 10, 2010.

For correspondence or reprints contact: Ming-Rong Zhang, Department of Molecular Probes, Molecular Imaging Center, National Institute of Radiological Sciences, 4-9-1 Anagawa, Inage-Ku, Chiba 263-8555, Japan.

E-mail: zhang@mirs.go.jp

COPYRIGHT © 2010 by the Society of Nuclear Medicine, Inc.

FEDAA1106), and *N*-benzyl-*N*-ethyl-2-(7-¹¹C-methyl-8-oxo-2-phenyl-7,8-dihydro-9H-purin-9-yl)acetamide (¹¹C-AC-5216) for the clinical investigation of TSPO in our institute (20–23). However, these PET ligands had little dissociation in the primate brain, which makes the assessment of their brain kinetics difficult (24–26). Thus, PET studies with ligands such as ¹¹C-AC-5216 create complications in the quantitative analysis of the measurement of TSPO expression and function in health and disease.

We recently synthesized two ¹⁸F-labeled oxopurine analogs: *N*-benzyl-*N*-ethyl-2-[7,8-dihydro-7-(2-¹⁸F-fluoroethyl)-8-oxo-2-phenyl-9H-purin-9-yl]acetamide (¹⁸F-FEAC) and *N*-benzyl-*N*-methyl-2-[7,8-dihydro-7-(2-¹⁸F-fluoroethyl)-8-oxo-2-phenyl-9H-purin-9-yl]acetamide (¹⁸F-FEDAC) (27). ¹⁸F-FEAC (inhibition constant [*K*_i], 0.2 nM) and ¹⁸F-FEDAC (*K*_i, 1.3 nM) had potent in vitro binding affinity for TSPO with high selectivity (*K*_i, >8,700 nM for central benzodiazepine receptor). A previous small-animal PET study for a neuroinflammatory rat model demonstrated that both ¹⁸F-ligands had high uptake of radioactivity in a kainic acid-infused striatum, a brain region where TSPO expression was augmented (27).

In this study, we performed in vitro autoradiography and small-animal PET to visualize elevated TSPO expression in infarcted rat brains and evaluate the potential of ¹⁸F-FEAC and ¹⁸F-FEDAC for the imaging of TSPO. We investigated the brain kinetics of both ¹⁸F-ligands and compared their uptake and kinetics with those of ¹¹C-AC-5216 in the same monkey. In addition, we determined biodistribution in whole mice and performed metabolite analysis in mouse brain and plasma and in monkey plasma using ¹⁸F-FEAC and ¹⁸F-FEDAC.

MATERIALS AND METHODS

Radioligands

¹⁸F-FEAC. For irradiation, 95% enriched ¹⁸O-H₂O was used. ¹⁸F was produced by the ¹⁸O(p,n)¹⁸F nuclear reaction using a CYPRIS HM-18 cyclotron (Sumitomo Heavy Industries). The radioactive intermediate ¹⁸F-FCH₂CH₂Br (22) was reacted with a precursor (1 mg) and NaOH (7 μL, 0.5N aqueous solution) in dimethylformamide (300 μL) at 90°C for 15 min. After purification by high-performance liquid chromatography (HPLC), 920–1,460 MBq (*n* = 23) of ¹⁸F-FEAC were obtained as an injectable solution at a beam current of 15 μA and proton bombardment of 15 min. The radiochemical purity and specific activity of ¹⁸F-FEAC were at least 98% and 290–420 GBq/μmol at the end of synthesis.

¹⁸F-FEDAC. The radiosynthesis procedure for ¹⁸F-FEDAC was similar to that for ¹⁸F-FEAC except that a different precursor was used. At the end of synthesis, 840–1,520 MBq (*n* = 25) of ¹⁸F-FEDAC were obtained with a radiochemical purity of at least 97% and specific activity of 330–450 GBq/μmol.

Animal Experiments

All animal experiments were performed according to the recommendations of the Committee for the Care and Use of Laboratory Animals, National Institute of Radiologic Sciences. Animals were maintained and handled in accordance with the recommendations of the National Institutes of Health and the

institutional guidelines of the National Institute of Radiologic Sciences.

Biodistribution Study on Mice

A saline solution of ¹⁸F-FEAC (1.7 MBq/200 μL, 350 GBq/μmol) or ¹⁸F-FEDAC (2.1 MBq/200 μL, 330 GBq/μmol) was injected into ddY mice (7 wk old, male) through the tail vein. At 1, 5, 15, 30, 60, and 90 min after injection, 3 mice per time point were sacrificed by cervical dislocation. Whole brain, heart, lung, liver, kidney, spleen, bone, muscle, small intestine, testicle, and blood samples were quickly removed and weighed carefully. The radioactivity in these tissues was measured using a 1480 Wizard γ-counter (Perkin-Elmer) and expressed as a percentage of the injected dose (%ID) per gram of wet tissue. All radioactivity measurements were corrected for decay.

In Vitro Autoradiography Study on Infarcted Rat Brains

Transient focal ischemia in rats was produced by intraluminal occlusion of the middle cerebral artery for 30 min using a 3-vessel occlusion/reperfusion model (5,18). After ischemic surgery, the filament was removed for reperfusion. During this process, no behavioral change was observed in these animals. The body temperature of these rats was monitored and maintained. The rats were used 7 d after the surgery.

The rats were sacrificed by decapitation under diethyl ether anesthesia, and the brains were quickly removed and frozen on powdered dry ice. Coronal brain sections (20 μm) were cut with a cryostat (HM560; Carl Zeiss) at –15°C. Brain sections were immersed in a buffer of 50 mM Tris(hydroxymethyl)aminomethane hydrochloride (Trizma; Sigma-Aldrich) for 20 min at 25°C. ¹⁸F-FEAC (320 GBq/μmol) or ¹⁸F-FEDAC (350 MBq/μmol) with the same radioactivity (3.7 MBq) was added to the incubation solutions. To determine the specific binding of each ¹⁸F-ligand to TSPO, we added AC-5216 or PK11195 (10 μM) to the incubation solutions in advance. Brain sections were incubated at 25°C for 30 min. After incubation, the sections were washed twice for 2 min each time with cold buffer, dipped in cold distilled water, and dried with cold air. These sections were then placed in contact with imaging plates (BAS-MS2025; Fujifilm). Autoradiograms were obtained and quantified using a Bio-Imaging Analyzer System (BAS5000; Fujifilm). Radioactivity concentrations in the brain regions were measured and expressed as photostimulated luminescence per area (mm²). Regions of interest (ROIs) were placed on the infarcted areas (10.3 ± 2.3 mm²/slice) of ipsilateral sides and the same areas of the contralateral sides. Finally, these sections were stained with cresyl violet.

Small-Animal PET Study on Infarcted Rat Brains

PET Scans. Anatomic template images of rat brains were generated by a high-resolution MRI system. Briefly, a rat was anesthetized with sodium pentobarbital (50 mg/kg, intraperitoneally) and scanned with a 40-cm-bore, 7-T horizontal magnet (NIRS/KOBELCO; Bruker BioSpin) equipped with 12-cm-diameter gradients (Bruker BioSpin). A 7.2-cm-diameter coil was used for radiofrequency transmission, and signals were received by a 4-channel surface coil. Coronal T2-weighted MR images were obtained by a fast spin-echo sequence with the following imaging parameters: repetition time, 8,000 min; effective echo time, 15 min; field of view, 3.5 × 3.5 cm; and slice thickness, 0.6 mm.

PET scans were performed using an Inveon small-animal PET scanner (Siemens Medical Solutions), which provides 159 trans-

axial slices 0.796 mm (center-to-center) apart, a 10-cm transaxial field of view, and a 12.7-cm axial field of view. Before the scans, the rats were anesthetized with 5% (v/v) isoflurane, and maintained thereafter by 1%–2% (v/v) isoflurane. After transmission scans for attenuation using a ^{57}Co point source, emission scans were performed for 60 min after the intravenous injection of each ^{18}F -ligand (17 ± 3 MBq, 310–400 GBq/ μmol). PET images were obtained by summing the uptake between 0 and 60 min. In pretreatment studies, unlabeled TSPO ligands (AC-5216, 1 mg/kg/2 mL, or PK11195, 3 mg/kg/2 mL; dissolved in distilled water containing 10% ethanol and 5% polysorbate 80) were injected 30 s before injection of ^{18}F -ligand (17 ± 2 MBq, 310–390 GBq/ μmol). Because pretreatment with AC-5216 or PK11195 affected the initial uptake of ^{18}F -ligand, PET images in this study were obtained by summing the uptake between 10 and 60 min after injection of ^{18}F -ligand.

All list-mode acquisition data were sorted into 3-dimensional sinograms, which were then Fourier-rebinned into 2-dimensional sinograms (frames \times min: 4×1 , 8×2 , 8×5). Dynamic images were reconstructed with filtered backprojection using a Ramp filter and a Nyquist cutoff of 0.5 cycle/pixel. ROIs were placed on the infarcted areas (9.2 ± 1.5 mm²/slice) of ipsilateral sides and the same areas of contralateral sides using ASIPro VM (Analysis Tools and System Setup/Diagnostics Tool; Siemens Medical Solutions) with reference to the MRI template. Each PET image for each ^{18}F -ligand was overlaid on the MR image in the rat brain, and a time–activity curve for each brain region was determined.

Brain uptake of radioactivity was decay-corrected to the injection time and expressed as the standardized uptake value, normalized for injected radioactivity and body weight: (radioactivity per cubic centimeter tissue/injected radioactivity) \times gram body weight.

PET Data Modeling. Binding potential relative to nondisplaceable binding (BP_{nd}) was estimated for the kinetics of the ipsilateral and contralateral ROIs using the PMOD software package (version 3.1; PMOD Technologies). The simplified reference-tissue model was used, and the contralateral mirrored ROI was used as the reference region to determine BP_{nd} . All statistical examinations in this PET study were performed using GraphPad Prism, version 5 (GraphPad Software Inc.).

PET Study on Monkey

PET was performed using a high-resolution SHR-7700 PET camera (Hamamatsu Photonics) designed for laboratory animals. This camera provides 31 transaxial slices 3.6 mm (center-to-center) apart and a 33.1-cm field of view. An MR image of the brain was obtained using a Gyroscan S15/ACS II (1.5 T; Philips) with a 3-dimensional T1-weighted axial MR image sequence. A male rhesus monkey (*Macaca mulatta*) weighing about 8 kg was anesthetized with ketamine (10 mg/kg/h, intramuscularly) every hour throughout the session. Transmission scans for attenuation correction were subsequently performed for 20 min using a 74-MBq ^{68}Ge – ^{68}Ga source. A dynamic transmission scan in the 3-dimensional acquisition mode was performed for 90 min (1 min \times 4 scans, 2 min \times 8 scans, 5 min \times 8 scans, 10 min \times 3 scans). Emission scan images were reconstructed with a Colsher filter of 4 mm, and circular ROIs with a 5-mm diameter were placed over the occipital cortex and frontal cortex using image analysis software (20). A solution of ^{11}C -AC-5216 (100 MBq, 140 GBq/ μmol), ^{18}F -FEAC (110 MBq, 380 GBq/ μmol), or ^{18}F -FEDAC (115 MBq, 350 GBq/ μmol) was injected into the monkey, and time-sequential tomo-

graphic scanning was performed for 90 min on a transverse section of the brain. ROIs were placed on the occipital cortex and frontal cortex using the image analysis software PMOD with reference to the MR image of the monkey brain. Each PET image for each ^{18}F -ligand was overlaid on the MR image in the monkey brain, and a time–activity curve for each brain region was determined. Brain uptake of radioactivity was decay-corrected to the injection time and expressed as %ID per volume (mL).

Metabolite Assay

Mouse Plasma and Brain. After intravenous injection of ^{18}F -ligand (5 MBq/200 μL , 330–380 GBq/ μmol) into ddy mice ($n = 4$), these mice were sacrificed by cervical dislocation at 1, 5, 15, 30 and 60 min. Blood (0.5–1.0 mL) and whole-brain samples were removed quickly. The blood sample was centrifuged at 15,000 rpm for 1 min at 4°C to separate plasma, 250 μL of which were collected in a test tube containing CH_3CN (500 μL) and unlabeled authentic sample (10 μL of a 1 mg/5.0 mL concentration of CH_3CN). After the tube was stirred in a vortex mixer for 15 s and centrifuged at 15,000 rpm for 2 min for deproteinization, the supernatant was collected. The extraction efficiency of radioactivity into the CH_3CN supernatant ranged from 84% to 96% of total radioactivity in the plasma. On the other hand, the cerebellum and forebrain were dissected from the mouse brain and homogenized together in ice-cooled 1:1 $\text{CH}_3\text{CN}/\text{H}_2\text{O}$ (1.0 mL) solution. The homogenate was centrifuged at 15,000 rpm for 2 min at 4°C, and the supernatant was collected. The recovery of radioactivity into the supernatant was more than 80% based on total radioactivity in the brain homogenate.

An aliquot of the supernatant (100–300 μL) prepared from the plasma or brain homogenate was injected into the analytic HPLC system (Capcell Pak C₁₈ [Shiseido Co., Ltd.], 4.6-mm internal diameter \times 250 mm, 254 nm; 1:1 $\text{CH}_3\text{CN}/\text{H}_2\text{O}$; 1.5 mL/min). The percentage ratio of intact ^{18}F -ligand to total radioactivity (corrected for decay) on the HPLC chromatogram was calculated as (peak area for ^{18}F -ligand/total peak area) \times 100.

Monkey Plasma. After intravenous injection of ^{18}F -ligand (110,130 MBq) into the monkey, arterial blood samples (1 mL) were collected at 2, 5, 15, 30, 60, and 90 min. All samples were centrifuged at 15,000 rpm for 1 min at 4°C to separate plasma, 250 μL of which were collected in a test tube containing CH_3CN (0.5 mL). The plasma was treated as described above.

RESULTS

Biodistribution Study on Mice

The radioactivity distribution of ^{18}F -FEAC and ^{18}F -FEDAC was measured over 90 min in mice. As shown in Table 1, both ^{18}F -ligands had a similar distribution pattern in the examined regions. High uptake (>5 %ID/g) was found in the lung, heart, and kidney, which are known to be TSPO-enriched organs. Subsequently, radioactivity in the lung and heart declined rapidly until 5 min and then decreased slowly until the end of the experiment. Uptake in the liver and kidney peaked at 5 min and then decreased slowly. In the blood, radioactivity decreased immediately after injection and remained low. High initial uptake (>1 % ID/g) was determined in the mouse brain, the target tissue in this study. No significant increase in radioactivity was detected in bone.

TABLE 1. Distribution in Mice

Ligand	Tissue	1 min	5 min	15 min	30 min	60 min	90 min	
¹⁸ F-FEAC	Blood	1.84 ± 0.38	0.85 ± 0.02	0.66 ± 0.00	0.67 ± 0.04	0.82 ± 0.17	0.73 ± 0.06	
	Heart	15.55 ± 1.42	9.59 ± 1.17	5.45 ± 0.14	3.51 ± 0.10	2.40 ± 0.20	2.09 ± 0.04	
	Lung	82.68 ± 14.71	35.27 ± 3.50	23.57 ± 2.52	16.47 ± 2.21	10.38 ± 1.23	8.18 ± 0.42	
	Liver	4.88 ± 0.92	9.28 ± 1.83	9.72 ± 0.58	7.12 ± 0.57	5.36 ± 0.31	4.60 ± 0.45	
	Spleen	2.32 ± 0.15	7.80 ± 1.13	8.83 ± 0.70	7.43 ± 0.72	5.35 ± 0.68	5.25 ± 0.16	
	Kidney	14.94 ± 1.56	17.09 ± 4.01	15.64 ± 0.55	11.96 ± 0.76	8.65 ± 0.66	7.48 ± 0.52	
	Small intestine	4.33 ± 0.59	5.44 ± 1.10	7.99 ± 1.04	13.96 ± 3.19	7.53 ± 1.52	7.08 ± 3.49	
	Testicle	0.46 ± 0.03	0.53 ± 0.10	0.69 ± 0.01	0.72 ± 0.05	0.80 ± 0.05	0.84 ± 0.02	
	Muscle	2.16 ± 0.75	1.80 ± 0.31	1.66 ± 0.26	1.34 ± 0.15	1.30 ± 0.11	1.10 ± 0.07	
	Bone	1.05 ± 0.45	1.35 ± 0.20	1.41 ± 0.17	1.21 ± 0.18	1.65 ± 0.19	1.40 ± 0.45	
	Brain	1.06 ± 0.09	0.69 ± 0.08	0.45 ± 0.05	0.40 ± 0.02	0.42 ± 0.02	0.45 ± 0.03	
	¹⁸ F-FEDAC	Blood	1.77 ± 0.16	0.82 ± 0.21	0.74 ± 0.14	0.72 ± 0.09	0.66 ± 0.02	0.45 ± 0.09
		Heart	15.29 ± 2.09	8.32 ± 0.80	5.71 ± 0.66	3.78 ± 0.31	2.40 ± 0.10	1.38 ± 0.17
		Lung	61.75 ± 4.49	27.75 ± 6.88	23.28 ± 4.17	16.77 ± 0.78	10.30 ± 0.54	6.59 ± 0.87
Liver		7.65 ± 1.98	10.29 ± 1.00	10.51 ± 1.29	10.36 ± 0.72	7.09 ± 0.46	4.65 ± 0.33	
Spleen		3.49 ± 1.41	5.57 ± 0.97	7.14 ± 0.94	7.43 ± 0.49	5.77 ± 0.39	3.86 ± 0.67	
Kidney		17.75 ± 3.17	15.49 ± 0.83	14.11 ± 1.46	14.40 ± 0.80	9.08 ± 0.45	5.63 ± 1.07	
Small intestine		5.84 ± 1.20	5.62 ± 0.11	7.14 ± 0.80	14.05 ± 7.43	9.57 ± 2.12	6.98 ± 3.15	
Testicle		0.51 ± 0.06	0.61 ± 0.14	0.72 ± 0.10	0.92 ± 0.14	0.81 ± 0.14	0.54 ± 0.16	
Muscle		2.38 ± 0.13	1.96 ± 0.32	2.01 ± 0.47	1.66 ± 0.21	1.27 ± 0.28	0.64 ± 0.21	
Bone		1.85 ± 0.88	1.78 ± 0.35	1.84 ± 0.44	2.18 ± 0.33	2.02 ± 0.44	1.33 ± 0.13	
Brain		1.00 ± 0.14	0.67 ± 0.10	0.45 ± 0.03	0.40 ± 0.04	0.33 ± 0.03	0.21 ± 0.05	

Data are %ID/g tissue (mean ± SD; *n* = 3).

In Vitro Autoradiography Study on Infarcted Rat Brains

After evaluation in normal mice, we visualized elevated levels of TSPO expression in the infarcted rat brain after ischemia using each ¹⁸F-ligand. At day 7 after ischemic surgery, infarction was observed on the ipsilateral side but not on the contralateral side. By cresyl violet staining, neuronal loss and gliosis were confirmed in the infarcted brain sections. Figure 1 shows the in vitro autoradiographic results. For each ¹⁸F-ligand, binding was higher on the ipsilateral side than on the contralateral side: the ratios of radioactivity between the 2 sides were 1.80 ± 0.2 (*n* = 4) for ¹⁸F-FEAC and 1.73 ± 0.3 (*n* = 4) for ¹⁸F-FEDAC. The difference in radioactivity between contralateral and ipsilateral sides was abolished by coinubation with an excess of AC-5216 or PK11195. These treatments reduced the radioactivity on the 2 sides. As shown in Figure 2G, the decrease in binding by AC-5216 was more significant on the ipsilateral side (75% decrease for ¹⁸F-FEAC and 73% for ¹⁸F-FEDAC) than on the contralateral side (56% for ¹⁸F-FEAC and 40% for ¹⁸F-FEDAC). PK11195 also inhibited the radioactivity level of each ¹⁸F-ligand on the ipsilateral and contralateral sides.

Small-Animal PET Study on Infarcted Rat Brains

Figures 2 and 3 show representative PET images and time-activity curves of ¹⁸F-FEAC and ¹⁸F-FEDAC, respectively, in the infarcted rat brain. PET images (Figs. 2A and 3A) displayed a contrast of radioactivity between ipsilateral and contralateral sides. Each ¹⁸F-ligand had higher uptake on ipsilateral sides than on contralateral sides. Their time-

activity curves (Figs. 2D and 3D) were similar in rat brains. Each ¹⁸F-ligand entered the brain rapidly, and the radioactivity level in the brain peaked within 1–3 min after injection. Maximum uptake on the ipsilateral and contralateral sides was about 0.87 and 0.49 standardized uptake value, respectively, for ¹⁸F-FEAC and 0.91 and 0.57 standardized uptake value, respectively, for ¹⁸F-FEDAC. Compared with the contralateral side, where radioactivity decreased rapidly after its low initial uptake, radioactivity on the ipsilateral side decreased slowly. At the end of the PET scan, the uptake decreased to 72% (¹⁸F-FEAC) and 66% (¹⁸F-FEDAC) of the corresponding maximum uptake on the ipsilateral side, respectively. The uptake ratios of radioactivity between ipsilateral and contralateral sides reached 3.03 for ¹⁸F-FEAC and 2.76 for ¹⁸F-FEDAC at 20 min after injection (Fig. 4). Time-activity curves were analyzed using the simplified reference-tissue model to estimate the BP_{nd} of each ¹⁸F-ligand. The BP_{nd} values were 1.70 ± 0.19 (*n* = 4) for ¹⁸F-FEAC and 1.37 ± 0.06 (*n* = 4) for ¹⁸F-FEDAC. This difference in BP_{nd} between ¹⁸F-ligands was statistically significant (*P* < 0.05, unpaired *t* test with Welch correction).

The effects of unlabeled TSPO ligands (AC-5216, 1 mg/kg; PK11195, 3 mg/kg) on the uptake and kinetics of each ¹⁸F-ligand were determined. As shown in their PET images (¹⁸F-FEAC: Figs. 2B and 2C; ¹⁸F-FEDAC: Figs. 3B and 3C) and time-activity curves (¹⁸F-FEAC: Figs. 2E and 2F; ¹⁸F-FEDAC: Figs. 3E and 3F), AC-5216 or PK11195 diminished the contrast of radioactivity between ipsilateral and contralateral sides. By pretreatment with these TSPO

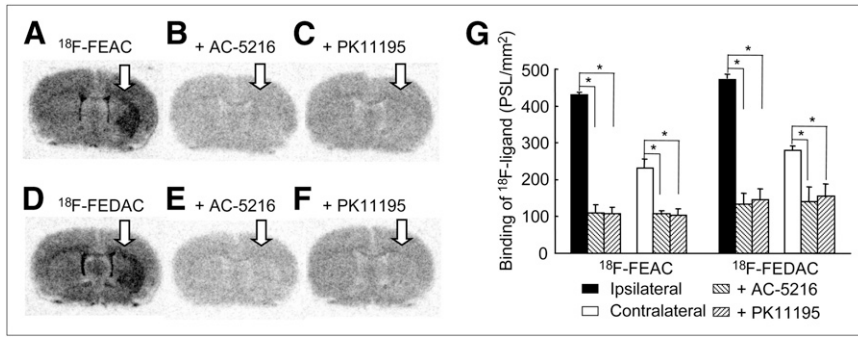


FIGURE 1. (A–F) Coronal autoradiographic results in infarcted rat brains, with arrows indicating infarcted areas: ^{18}F -FEAC (A), ^{18}F -FEAC with AC-5216 (B), ^{18}F -FEAC with PK11195 (C), ^{18}F -FEDAC (D), ^{18}F -FEDAC with AC-5216 (E), and ^{18}F -FEDAC with PK11195 (F). (G) Radioactivity concentration (photostimulated luminescence/mm 2 ; mean \pm SD, $n = 4$) was determined in these regions. * $P < 0.001$, compared with contralateral side in each group by Student paired t test.

ligands, the uptake ratio of each ^{18}F -ligand between the 2 sides was reduced to 1.0–1.4 (Fig. 4).

PET Study on Monkey

The uptake and kinetics of ^{18}F -FEAC and ^{18}F -FEDAC in the monkey brain were examined using PET. For comparison, PET with ^{11}C -AC-5216 was preliminarily performed for the same monkey. Figure 5 shows the summation images and time–activity curves of the 3 PET ligands in the monkey brain. Like ^{11}C -AC-5216, ^{18}F -FEAC and ^{18}F -FEDAC displayed a near-homogeneous pattern in the monkey brain. As seen from time–activity curves in the occipital cortex, the maximum uptake of ^{18}F -FEDAC (0.02% dose/mL) immediately after injection was similar to that of ^{11}C -AC-5216 at about 20 min and was higher than that of ^{18}F -FEAC (0.016% dose/mL) at 5 min. After reaching the maximum, the uptake of ^{11}C -AC-5216 maintained that level until the end of the PET scan. In contrast to ^{11}C -AC-5216, each ^{18}F -ligand showed decreased uptake over time in the brain. At 90 min after injection, the radioactivity of ^{18}F -FEAC and ^{18}F -FEDAC decreased to 70% and 61%, respectively, of the maximum. The uptake of each ^{18}F -ligand decreased with time in the occipital cortex and in

the frontal cortex, striatum, thalamus, and cerebellum of the monkey brain.

As seen on the PET images, no significant accumulation of radioactivity was observed in the monkey skull during the scan with each ^{18}F -ligand.

Metabolite Analysis

Figure 6 shows the percentages of unmetabolized ^{18}F -ligand in the plasma and brain homogenate of mice analyzed by radio-HPLC. After injection into the mice, the fraction corresponding to intact ^{18}F -ligand in the plasma decreased over time. In the brain homogenate, the percentages of intact ^{18}F -FEAC and ^{18}F -FEDAC were 68% and 75% at 30 min after injection, respectively. A radioactive metabolite with high polarity was observed on the HPLC chart of each ^{18}F -ligand.

Table 2 shows the results of metabolite analysis in monkey plasma. The fraction corresponding to the unmetabolized ^{18}F -FEAC and ^{18}F -FEDAC in the plasma remained at 96% of the total radioactivity at 30 min after injection. The percentages of intact forms were 87% and 80%, respectively, for ^{18}F -FEAC and ^{18}F -FEDAC at the end (90 min) of the PET scans. Only a small amount of the same radiolabeled metabolite of each ^{18}F -ligand was detected.

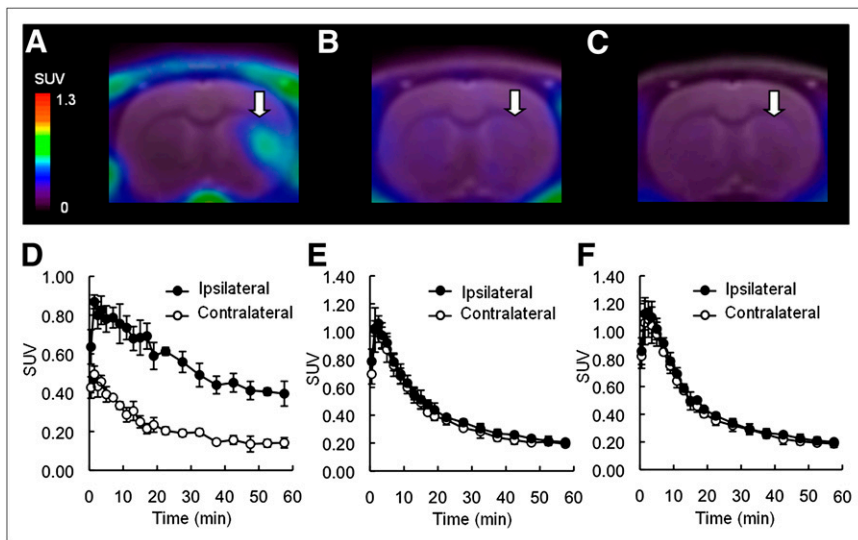


FIGURE 2. Representative PET images and time–activity curves of ^{18}F -FEAC in infarcted rat brains. PET images were generated by averaging whole scan and were overlaid on MR images. Arrows indicate infarcted areas. Shown are control rats ($n = 4$) (A and D), rats pretreated with AC-5216 ($n = 4$) (B and E), and rats pretreated with PK11195 ($n = 4$) (C and F).

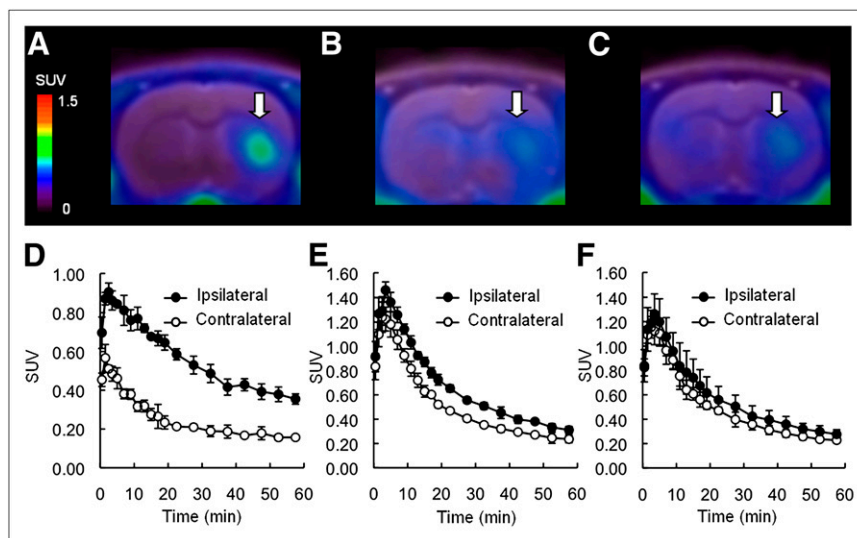


FIGURE 3. Representative PET images and time-activity curves of ^{18}F -FEDAC in infarcted rat brains. PET images were generated by averaging whole scan and were overlaid on MR images. Arrows indicate infarcted areas. Shown are control rats ($n = 4$) (A and D), rats pretreated with AC-5216 ($n = 4$) (B and E), and rats pretreated with PK11195 ($n = 4$) (C and F).

DISCUSSION

Although several dozen PET ligands have been developed for in vivo TSPO imaging (10,11), radioligands such as ^{11}C -AC-5216, ^{11}C -DAA1106, and ^{18}F -FEDAA1106 had little dissociation in the primate brain (23–26). The slow kinetics of these PET ligands is a significant disadvantage. The present study demonstrated that, compared with ^{11}C -AC-5216, ^{18}F -FEAC and ^{18}F -FEDAC had improved kinetics in the monkey brain. Both ^{18}F -ligands produced signals to allow in vitro and in vivo visualization of elevated TSPO expression in the infarcted rat brain.

Uptake of ^{18}F -FEAC and ^{18}F -FEDAC in normal mice agreed with the distribution of TSPO in rodents as reported previously (Table 1) (21,23). The highest uptake of radioactivity was in the lung and heart and may have been due to the high mitochondrial content of TSPO in these organs. Both ^{18}F -ligands had a relatively high level ($>1\%$ ID/g) of radioactivity in the brain, revealing that they could pass the blood–brain barrier and enter the brain rapidly—a prerequisite for a favorable PET ligand in brain imaging. Uptake in the brain may be related to the suitable lipophilicity of these ligands (calculated distribution coefficient ClogD : 3.6 for ^{18}F -FEAC and 3.2 for ^{18}F -FEDAC) (27).

Because of the relatively low density of TSPO in the normal rodent brain, we used an ischemic model to validate the usefulness of ^{18}F -FEAC and ^{18}F -FEDAC for in vitro and in vivo TSPO imaging. This is a well-known rat model in which TSPO expression is elevated by neuroinflammation with microglial activation in the infarcted areas of the brain (5,18). In vitro autoradiography showed that the ipsilateral side gave rise to a TSPO-rich area that could be readily and similarly visualized using ^{18}F -FEAC or ^{18}F -FEDAC (Fig. 1). Treatment with TSPO-specific ligands, AC-5216 or PK11195, blocked their binding on the ipsilateral and contralateral sides, suggesting that both ^{18}F -ligands had in vitro TSPO-specific binding in both inflammatory and noninflammatory areas of the infarcted brains.

In a small-animal PET study on infarcted brains, PET summation images showed a significant contrast of radioactivity between contralateral and ipsilateral sides (Figs. 2A and 3A). The uptake ratio of each ^{18}F -ligand between the 2 sides peaked at 20 min after injection. This ratio was significantly reduced by pretreatment with AC-5216 or PK11195 (Fig. 4). These results indicated that the in vivo binding of both ^{18}F -ligands was specific to TSPO and that increased binding was caused by overexpression of TSPO in the infarcted brains. The increase in the initial uptake of ^{18}F -ligand by pretreatment with AC-5216 (Figs. 2E and 3E)

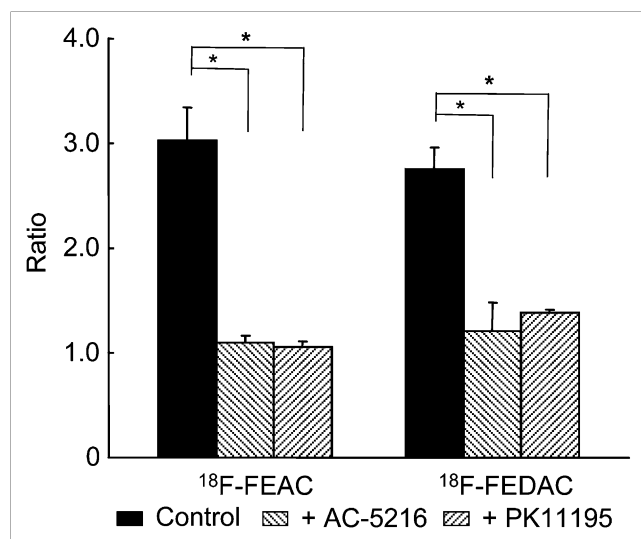


FIGURE 4. Uptake ratios (mean \pm SD, $n = 4$) between ipsilateral and contralateral sides of infarcted rat brains. Ratio was calculated from uptake data of ^{18}F -FEAC or ^{18}F -FEDAC at 20 min after injection. $*P < 0.001$, compared with control group (^{18}F -FEAC or ^{18}F -FEDAC only) in each group (pretreatment with AC-5216 or PK11195) by Student paired t test.

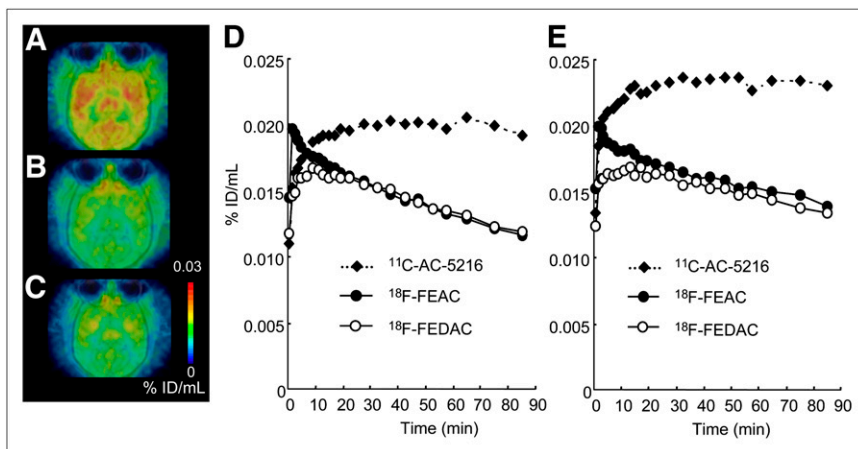


FIGURE 5. (A–C) PET images showing distribution of ^{11}C -AC-5216 (A), ^{18}F -FEAC (B), and ^{18}F -FEDAC (C) in brain of same rhesus monkey. These images were generated by averaging whole scan and were overlaid on MR images. (D and E) Time-activity curves for ^{11}C -AC-5216, ^{18}F -FEAC, and ^{18}F -FEDAC in occipital (D) and frontal cortex (E) of monkey brain.

or PK11195 (Figs. 2F and 3F) could be explained by precluding radioactivity from peripheral organs, because high radioactivity relative to TSPO binding was present in organs such as the lung and heart. Likely caused by the flow of radioactivity from the peripheral organs to the brain, the uptake ratio of ^{18}F -FEDAC between ipsilateral and contralateral sides was not reduced to 1 by pretreatment with AC-5216 or PK11195 (Fig. 4). On the other hand, the BP_{nd} value of ^{18}F -FEAC was slightly higher than that of ^{18}F -FEDAC, which might be due to the higher binding affinity of FEAC (K_i , 0.49 nM) than of FEDAC (1.34 nM) for TSPO (27).

To evaluate the potential of both ^{18}F -ligands in the primate brain, we compared the distribution pattern and kinetics of ^{18}F -FEAC and ^{18}F -FEDAC with those of ^{11}C -AC-5216 in the same monkey brain (Fig. 5). PET images showed that the distribution patterns of both ^{18}F -ligands were consistent with that of ^{11}C -AC-5216 in the monkey brain and were also similar to those of ^{11}C -AC-5216 in the human brain, reported previously (26). This result, in addition

to the structural similarity of the 3 radioligands, confirmed that the uptake of both ^{18}F -ligands reflected the distribution of TSPO in the monkey brain. The maximum uptake of ^{18}F -FEAC and ^{18}F -FEDAC in the occipital cortex, frontal cortex, and other regions of the monkey brain were 3–4 times higher than that of ^{11}C -PK11195 in the same monkey, as calculated from our previous studies (20). The radioactivity of ^{18}F -FEDAC in the brain peaked immediately after injection and then decreased. ^{18}F -FEAC also displayed a slow decrease in the brain after the maximum level had been reached at 5 min. In contrast to both ^{18}F -ligands, ^{11}C -AC-5216, like ^{11}C -DAA1106 and ^{18}F -FEDAA1106, did not dissociate in any brain regions (23). The kinetics of both ^{18}F -ligands in the monkey brain may be preferable to those of ^{11}C -AC-5216 for PET assessment.

The relatively rapid kinetics may be due to the decreased binding affinity of both ^{18}F -ligands with TSPO. FEDAC and FEAC displayed slightly lower affinities with TSPO (K_i , 1.34 and 0.49 nM, respectively) than did AC-5216 (0.20 nM), DAA1106 (0.16 nM), and FEDAA1106 (0.08 nM). Reduction of the binding affinity may result in the dissociation of both ^{18}F -ligands from TSPO in the brain. FEAC (cLogD, 3.6) and FEDAC (3.2) became less lipophilic than did DAA1106 (3.7) and FEDAA1106 (3.8)—a characteristic that could reduce nonspecific binding in the brain. Thus, suitable lipophilicity may also partly contribute to the clearance of both ^{18}F -ligands in the brain.

As seen from the PET summation images (Figs. 2, 3, and 5), no significant accumulation of $^{18}\text{F}\text{-F}^-$ was observed in

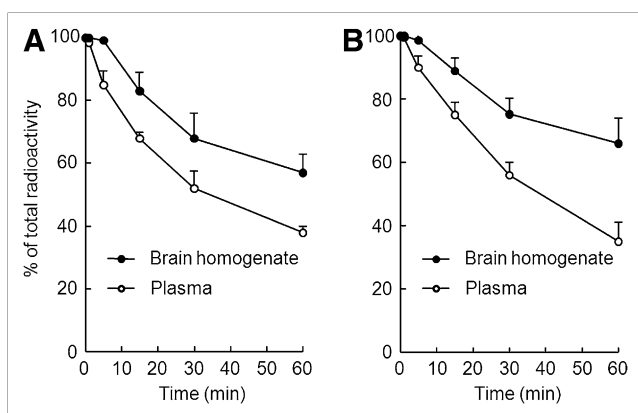


FIGURE 6. Percentages (mean \pm SD, $n = 4$) of unmetabolized ^{18}F -ligand in mouse plasma and brain homogenate at several time points after injection of ^{18}F -ligand: ^{18}F -FEAC (A) and ^{18}F -FEDAC (B).

TABLE 2. Percentages of Intact ^{18}F -Ligand in Monkey Plasma

Time (min)	^{18}F -FEAC (%)	^{18}F -FEDAC (%)
1	99.8	99.3
5	98.6	99.1
15	97.8	98.8
30	96.4	96.1
60	90.2	85.7
90	86.5	79.8

the skulls of rat and monkey. Distribution in mice by the dissection method also demonstrated no significant radioactivity in bones (Table 1). On the other hand, although the radiolabeled metabolite of each ^{18}F -ligand was found in the brain homogenate of mice, intact ^{18}F -ligand was represented as the main component (Fig. 6). The percentage of intact ^{18}F -FEAC or ^{18}F -FEDAC was 83% or 89% in the homogenate at 15 min after injection, but the maximum uptake ratio of each ^{18}F -ligand between ipsilateral and contralateral sides was achieved within 15–20 min. These results indicated that the specific binding of ^{18}F -FEAC or ^{18}F -FEDAC with TSPO in the infarcted rat brain was mainly due to these radioligands themselves. Further, in vivo metabolite analysis confirmed the relative stability of each ^{18}F -ligand in the monkey plasma (Table 2). Thus, PET for TSPO in the primate brain was unlikely to be affected by their radiolabeled metabolites.

The present PET results suggested that ^{18}F -FEAC and ^{18}F -FEDAC are useful for in vivo imaging and quantification of TSPO in the brain. Based on their kinetics in the brain, a PET study using both ^{18}F -ligands may be suitable for quantitative analysis of the expression and change in TSPO, in comparison with ^{11}C -AC-5216. Although these ^{18}F -ligands with relatively rapid dissociation may show limited specificity for TSPO, and their brain kinetics may be easily influenced by blood flow, it is worth comparing their kinetics and BP_{nd} with those of ^{11}C -AC-5216 in the human brain. Whether the elevated TSPO expression in the neuroinflammatory brains could be detected efficiently using both ^{18}F -ligands needs to be elucidated. Recently, some TSPO PET ligands, such as the pyrazolopyrimidine analogs ^{11}C -DPA-713 and ^{18}F -DPA-714, have already shown suitable kinetics in the primate brain (14,15,17,18). It would be valuable to compare the oxopurine analogs ^{18}F -FEAC and ^{18}F -FEDAC with pyrazolopyrimidine and other structure radioligands using the same experimental animal model prepared under the same conditions.

CONCLUSION

^{18}F -FEAC and ^{18}F -FEDAC provided sufficient signals to allow visualization of TSPO in infarcted rat brains in vitro and in vivo. The kinetics in the monkey brain and tolerance for in vivo metabolism suggest their usefulness for imaging studies of TSPO in normal and abnormal brains. Thus, the prospects for human clinical investigations using both ^{18}F -ligands are promising. We expect that in vivo TSPO imaging in humans can be used to quantitatively estimate the neuroinflammation and outcomes of disease-modifying treatments in neurodegenerative disorders such as Alzheimer disease.

ACKNOWLEDGMENTS

We thank Takashi Okauchi and Hidekatsu Wakisaka (National Institute of Radiological Sciences) for their help with PET scans. We also thank the staff of the National

Institute of Radiological Sciences for their help with radiosynthesis and animal experiments. This study was supported in part by a Grant-in-Aid for the Molecular Imaging Program from the Ministry of Education, Culture, Sports, Science and Technology, Government of Japan.

REFERENCES

1. Papadopoulos V, Baraldi M, Guilarte TR, et al. Translocator protein (18kDa): new nomenclature for the peripheral-type benzodiazepine receptor based on its structure and molecular function. *Trends Pharmacol Sci.* 2006;27:402–409.
2. Braestrup C, Albrechtsen R, Squires RF. High densities of benzodiazepine receptors in human cortical areas. *Nature.* 1977;269:702–704.
3. Gavish M, Bachman I, Shoukrun R, et al. Enigma of the peripheral benzodiazepine receptor. *Pharmacol Rev.* 1999;51:629–650.
4. Maeda J, Higuchi M, Inaji M, et al. Phase-dependent roles of reactive microglia and astrocytes in nervous system injury as delineated by imaging of peripheral benzodiazepine receptor. *Brain Res.* 2007;1157:100–111.
5. Rojas S, Martin A, Arranz MJ, et al. Imaging brain inflammation with [^{11}C]PK11195 by PET and induction of the peripheral-type benzodiazepine receptor after transient focal ischemia in rats. *J Cereb Blood Flow Metab.* 2007;27:1975–1986.
6. Chen MK, Guilarte TR. Translocator protein 18kDa (TSPO): molecular sensor of brain injury and repair. *Pharmacol Ther.* 2008;118:1–17.
7. Maeda J, Ji B, Irie T, et al. Longitudinal, quantitative assessment of amyloid, neuroinflammation, and anti-amyloid treatment in a living mouse model of Alzheimer's disease enabled by positron emission tomography. *J Neurosci.* 2007;27:10957–10968.
8. Yasuno F, Ota M, Kosaka J, et al. Increased binding of peripheral benzodiazepine receptor in Alzheimer's disease measured by positron emission tomography with [^{11}C]DAA1106. *Biol Psychiatry.* 2008;64:835–841.
9. Ji B, Maeda J, Sawada M, et al. Imaging of peripheral benzodiazepine receptor expression as biomarkers of detrimental versus beneficial glial responses in mouse models of Alzheimers and other CNS pathologies. *J Neurosci.* 2008;28:12255–12267.
10. Chauveau F, Boutin H, Van Camp N, Dollé F, Tavittian B. Nuclear imaging of neuroinflammation: a comprehensive review of [^{11}C]PK11195 challengers. *Eur J Nucl Med Mol Imaging.* 2008;35:2304–2319.
11. Dollé F, Luus C, Reynolds A, Kassiou M. Radiolabelled molecules for imaging the translocator protein (18 kDa) using positron emission tomography. *Curr Med Chem.* 2009;16:2899–2923.
12. Brown AK, Fujita M, Fujimura Y, et al. Radiation dosimetry and biodistribution in monkey and man of ^{11}C -PBR-28: a PET ligand to image inflammation. *J Nucl Med.* 2007;48:2072–2079.
13. Fookes CJ, Pham TQ, Mattner F, et al. Synthesis and biological evaluation of substituted [^{18}F]imidazo[1,2-a]pyridines and [^{18}F]pyrazolo[1,5-a]pyrimidines for the study of the peripheral benzodiazepine receptor using positron emission tomography. *J Med Chem.* 2008;51:3700–3712.
14. James ML, Fulton RR, Vercoullie J, et al. DPA-714, a new translocator protein-specific ligand: synthesis, radiofluorination, and pharmacological characterization. *J Nucl Med.* 2008;49:814–822.
15. Chauveau F, Van Camp N, Dollé F, et al. Comparative evaluation of the translocator protein radioligands ^{11}C -DPA-713, ^{18}F -DPA-714, and ^{11}C -PK11195 in a rat model of acute neuroinflammation. *J Nucl Med.* 2009;50:468–476.
16. Fujimura Y, Zoghbi SS, Simeon FG, et al. Quantification of translocator protein (18kDa) in the human brain with PET and a novel radioligand, ^{18}F -PBR06. *J Nucl Med.* 2009;50:1047–1053.
17. Endres CJ, Pomper MG, James M, et al. Initial evaluation of ^{11}C -DPA-713, a novel TSPO PET ligand, in humans. *J Nucl Med.* 2009;50:1276–1282.
18. Martin A, Boisgard R, Thézé B, et al. Evaluation of the PBR/TSPO radioligand [^{18}F]DPA-714 in a rat model of focal cerebral ischemia. *J Cereb Blood Flow Metab.* 2010;30:230–241.
19. Pappata S, Cornu P, Samson Y, et al. PET study of carbon-11-PK11195 binding to peripheral type benzodiazepine sites in glioblastoma: a case report. *J Nucl Med.* 1991;32:1608–1610.
20. Maeda J, Suhara T, Zhang MR, et al. Peripheral benzodiazepine receptor ligand [^{11}C]DAA1106 for PET: an imaging tool for glial cells in the brain. *Synapse.* 2004;52:283–291.
21. Zhang MR, Kida T, Noguchi J, et al. [^{11}C]DAA1106: radiosynthesis and in vivo binding to peripheral benzodiazepine receptors in mouse brain. *Nucl Med Biol.* 2003;30:513–519.

22. Zhang MR, Maeda J, Ogawa M, et al. Development of a new radioligand, N-(5-fluoro-2 phenoxyphenyl)-N-(2-[¹⁸F]fluoroethoxy-5-methoxybenzyl)acetamide, for PET imaging of peripheral benzodiazepine receptor in primate brain. *J Med Chem.* 2004;47:2228–2235.
23. Zhang MR, Kumata K, Maeda J, et al. [¹¹C]AC-5216: a novel positron emission tomography ligand for peripheral-type benzodiazepine receptors in primate brain. *J Nucl Med.* 2007;48:1853–1861.
24. Ikoma Y, Yasuno F, Ito H, et al. Quantitative analysis for estimating binding potential of the peripheral benzodiazepine receptor with [¹¹C]DAA1106. *J Cereb Blood Flow Metab.* 2007;27:173–184.
25. Fujimura Y, Ikoma Y, Yasuno F, et al. Quantitative analyses of [¹⁸F]FEDAA1106 binding to peripheral benzodiazepine receptors in living human brain. *J Nucl Med.* 2006;47:43–50.
26. Miyoshi M, Ito H, Arakawa R, et al. Quantitative analysis of peripheral benzodiazepine receptor in the human brain using PET with ¹¹C-AC-5216. *J Nucl Med.* 2009;50:1095–1101.
27. Yanamoto K, Kumata K, Yamasaki T, et al. [¹⁸F]FEAC and [¹⁸F]FEDAC: two novel positron emission tomography ligands for peripheral-type benzodiazepine receptor in brain. *Bioorg Med Chem Lett.* 2009;19:1707–1710.